Natural Hazards (2024) 120:8209–8238
https://doi.org/10.1007/s11069-023-06327-w

ORIGINAL PAPER

Discovery of imbricated beachrock deposits adjacent to the Java trench, Indonesia: influence of tsunami and storm waves, and implications for mega-thrust earthquakes

R. Harris[1] · W. Meservy[1] · H. Sulaeman[1] · M. Bunds[2] · J. Andreini[2] · B. Sharp[1] · B. Berrett[3] · J. Whitehead[4] · G. Carver[4] · G. Setiadi[5] · S. Hapsoro[5] · C. Prasetyadi[5]

Received: 21 March 2023 / Accepted: 22 June 2023 / Published online: 10 June 2024

Abstract

We discovered several imbricate beachrock deposits (IBD), one of which was observed to have formed during the tsunami caused by the 1994 7.8 Mw earthquake in East Java, Indonesia. Similar IBD were also found along the southern coastlines of central Java, Bali, Lombok, Sumba, Kisar, Leti and Nailaka Islands. Most IBD are composed of thin, rectangular ($2.5 \times 1.7 \times 0.4$ m) slabs of in situ calcareous beachrock dislodged from the intertidal platform during powerful wave impacts. The largest imbricated beachrock slabs are around 3 m^3. Ages of coral boulders incorporated into the IBD generally match with historical records of known tsunamigenic earthquakes and candidate paleotsunami sand deposit ages. To test for the influence of storms on the IBD, we measured the positions of boulders over a 3-year period at one site by overlaying digital surface models created from small uncrewed aerial system surveys. During the 3 years there were multiple uncommonly high wave events including two tropical cyclones, which are rare in Indonesia. Of the approximately 1220 slabs in the IBD around 113 moved slightly or flipped within the deposit, but no beachrock slabs were added or removed. The combination of data from various sources (eyewitnesses, consistent boulder characteristics, lack of storms or their effects on boulders, and age analyses) favors the hypothesis that the IBD are emplaced by recurring large wave events. The most probable causes of these events are tsunamis generated by the Java Trench and other submarine faults and landslides. If this is the case, then the IBD may provide durable records of previous mega-thrust earthquakes and tsunamis that should be incorporated into tsunami risk assessments for the highly populated coastlines of the eastern Sunda and Banda Arcs. We include two tsunami models that estimate > 6 million people inhabit likely inundation zones of a worst-case scenario tsunami generated by a Java Trench mega-thrust earthquake.

Keywords Tsunami hazards · Coastal boulder deposits · Beachrock · Java trench · Mega-thrust earthquakes · Tsunami modeling · Indonesia

Extended author information available on the last page of the article

1 Introduction

The Sunda Arc extends for 3200 km from offshore the Andaman Islands and Sumatra in the NW to Java and the Lesser Sunda Islands to the SE (Fig. 1). Historical and instrumental records document several mega-thrust earthquakes on the northern section of the Sunda Arc (Newcomb and McCann 1984; Harris and Major 2016; Martin et al. 2022). A Mw = 9.2 mega-thrust event occurred on this section in 2004, which claimed around 230,000 lives mostly due to the mega-tsunami it produced (e.g., Lay et al. 2005). Although historical accounts from Dutch colonists in Indonesia reach back to 1584, there is scarce evidence that the SE section of the Sunda Arc, the Java Trench, has experienced mega-thrust earthquakes like those well documented in Sumatra during the past 439 years.

Are these two parts of the Sunda Arc deforming in different ways? For example, does the Java Trench have a significant component of creep that explains the lack of instrumental earthquakes > Mw 7.8 (Newcomb and McCann 1984) or unequivocal mega-thrust earthquakes in historical records (Harris and Major 2016)? Alternatively, is the Java Trench in a strain accumulation phase that exceeds the time window of historical accounts? If the latter is the case, then the seismic and tsunami risk is likely very high for one of the world's most densely populated coastal areas facing a loaded subduction zone.

If the Java Trench, which has a convergent rate of 70 mm/a (Nugroho et al. 2009), is in an elastic strain buildup phase lasting > 439 years, then it has accumulated at least 30 m of potential slip over a broad area that could produce a Mw 8.8–9.1 event depending on possible rupture lengths of 500–1200 km, respectively. At the current state of seismic and tsunami readiness (Hall et al. 2017), this event could claim as many or more lives than the 2004 megathrust earthquake of the northern Sunda Arc.

To test whether mega-thrust earthquakes and large tsunamis along the Java Trench predate available historical accounts or are not recognized as such, we investigated geological records of paleotsunami deposits along the southern coast of Java, Bali, and islands of the eastern Sunda Arc (Figs. 1, 2). Candidate paleo-tsunami deposits include high-energy marine sand deposits in low-energy, terrestrial depositional environments, and may also

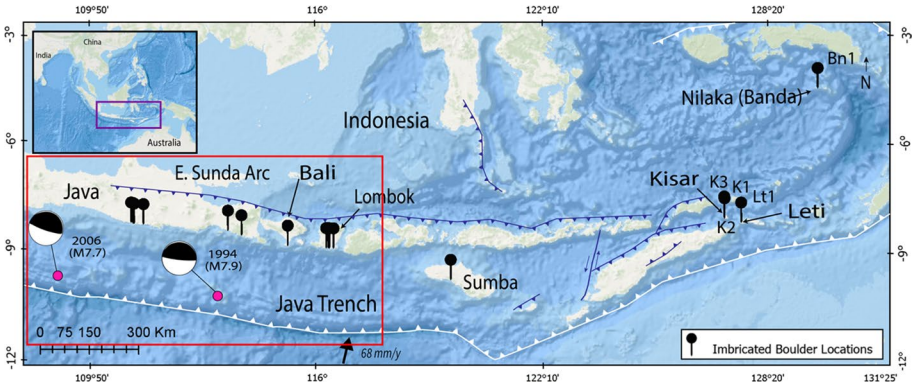

Fig. 1 Top left—Location map of Sunda Arc with rectangle showing position of large map. Large map shows parts of Java, Bali and the Lesser Sunda Islands (Lombok and islands to the east) with IBD occurrences and major tectonic features associated with Australian and Asian Plate convergence. Thrust faults have teeth on the upper plate. Black pins are IBD sites with site numbers for those outside the red box. Fault plane solutions are for the only instrumental earthquakes on the Java Trench subduction zone interface. Red box is approximate location of detailed map with site numbers for Java, Bali and Lombok (Fig. 2)

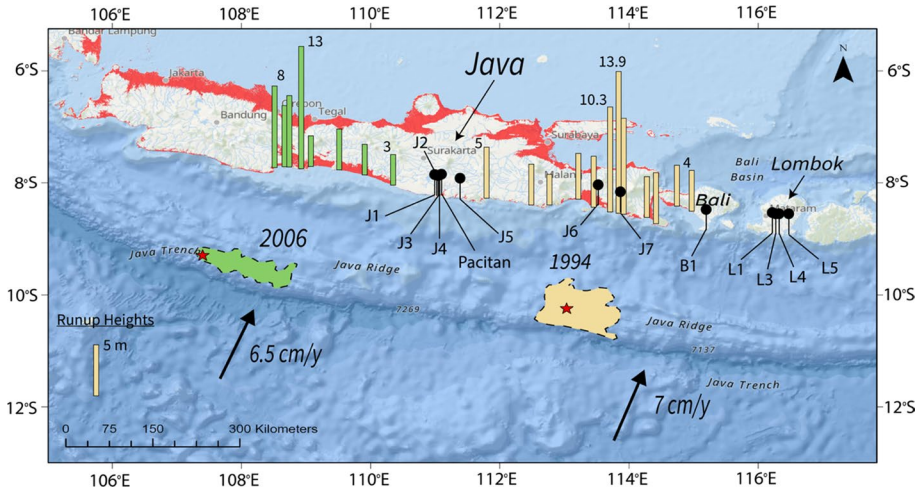

Fig. 2 Map of Java Trench and eastern Sunda Arc detailing IBD site locations in Java, Bali, and Lombok (black pins with site numbers). Green and tan patches are subduction interface rupture zones of the 2006 and 1994 earthquakes, respectively. Bars are runup heights of tsunamis caused by the earthquakes. Red coastal areas are < 30 m above sea level. Black arrows are plate convergence vectors

include distinct Imbricated Beachrock Deposits (IBD). *This paper focuses on the later, the origin and evolution of IBD adjacent to the Java Trench and possible connections to past mega-thrust earthquakes.*

1.1 Debate of coastal boulder deposit origins

The surface of the Indian Ocean stretches virtually unimpeded from Antarctica to the southern shores of the Sunda Arc, a distance that facilitates generation of high waves, especially at high spring tides. These waves contribute to significant coastal erosion in the region (Hastuti et al. 2022), which are associated with erosion of in situ beachrock outcrops in the intertidal zone. This erosion can form detached beachrock slabs in the intertidal zone (e.g., Cooper et al. 2019). Mechanisms of movement and imbrication of these slabs are controversial (Cox et al., 2018; Marriner et al. 2017; Vött et al. 2019). Some argue that imbrication of large rock slabs is likely a phenomenon of storm waves, which are much more common and ubiquitous than tsunamis (e.g., Kennedy et al 2021). Others argue that most coastal boulder deposits are formed by tsunamis due to the size and orderly stacking of the boulders (e.g., Scheffers 2008). However, it is difficult to interpret the mechanism from the IBD landform itself (e.g., Etienne & Paris 2010; Switzer and Burston 2010; Goto et al. 2012). Storm waves typically have periods of 5–20 s (wavelengths of 100–200 m), whereas tsunami wave trains are estimated to move at high velocities of 20–83 m/s across the continental shelf and 10–20 m/s near the shore, have periods from 10 to 120 min, and wavelengths around 500 km (e.g., Kato et al. 1991, 1995; Goto et al. 2009a, b). Another possibility, which we have not addressed in this study is the potential for surf-beat or infragravity waves (Roeber and Bricker 2015; Soria et al 2018) to produce IBD. However, because beachrock forms commonly in many locations, IBDs formed by these waves should be ubiquitous everywhere where there is a shallowing of the continental shelf

and/or where storms impact. Since we do not see large fields of IBDs everywhere where beachrock forms and these other conditions are present, it seems unlikely that the mechanism of formation is infragravity waves.

1.2 Imbricate beachrock deposits (IBD)

IBD are a type of coastal boulder deposit where the 'boulders' consist mostly of overlapping, tabular (tile-like) beachrock slabs (Fig. 3). Most beachrock is documented in mid-low latitude coastal regions and beaches with low tidal variation (Vousdoukas et al. 2007). Cementation of the beachrock mostly happens in the vadose zone during low tide when the sand deposits are exposed to the atmosphere. The lithification process is related to cementation of carbonate from fresh water (calcite) or sea water (aragonite) in the intertidal zone. Some studies show a strong correlation between beachrock formation and proximity to carbonate-rich shorelines (e.g., Russell 1962). All of the beachrock outcrops we discovered are near onshore carbonate outcrops.

Layered beachrock outcrops are autochthonous to the beach and dip seaward (Fig. 3) up to 10° steeper than the beach angle (e.g., Russell 1963; Davies and Kinsey, 1973). The majority of beachrock dated globally is 1000–5000 years old. However, these ages are skewed in an older direction due to lack of age data from modern beachrock (e.g., Scoffin 1993).

IBD demonstrate how beachrock slabs are excavated from joint-bounded outcrops and carried landward until encountering an obstacle or backstop (Fig. 3) where they stack up (Goff et al. 2010; Schiffers and Kinis 2014; Cox et al. 2019). Some slabs make it over the backstop onto the coastal plain inland from the IBD ridge (Fig. 3). The presence of these boulders document large enough waves to not only inundate the coastal plain but also to carry 2-m wide beachrock slabs there as well. These are processes not observed during annual or uncommon storm wave activity in Indonesia or in small seas not in the cyclonic zones such as Greece, which has multiple IBD (e.g., Boulton and Whitworth 2018).

The size and shape of IBD (Table 1) are characterized by a 3-axis system where the long axis (a) is commonly subparallel to the strike of the shoreline, the intermediate length axis (b) is parallel to the boulder transport direction, and the short axis (c) is the thickness of the slab (Nott 2000; Galvin 2003). These dimensions can be used to determine a flatness index '*Fb*', where $Fb = (a+b)/2c$ (Cailleux and Tricart, 1959). A value of 1 is a square or

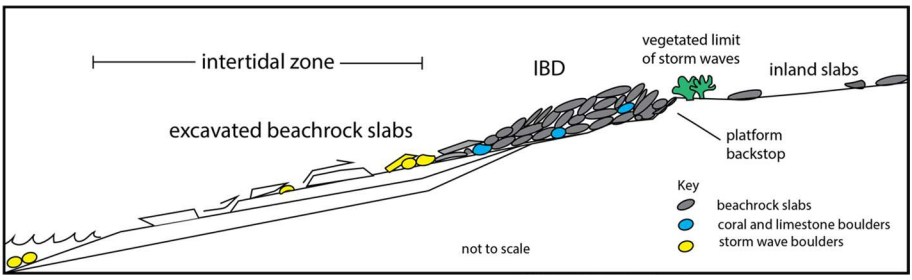

Fig. 3 Sketch of erosional and depositional settings of IBD in Indonesia. Layered beachrock (white) is torn from intertidal outcrops and stack up as imbricated slabs (gray) against a wave cut step or backstop at the rear of the supra-tidal platform. Blue—are coral boulders interlayered with IBD used for age constraints. Yellow—bedrock boulders deposited by storm waves. The view is parallel to the long axis of imbricated beachrock slabs

Table 1 Location and characteristics of IBD

Place/ beach	Site	Latitude	Longitude	*a*-axis (m)	*b*-axis (m)	*c*-axis (m)	[a]Fb	Area (m^2)	Elev (m)
Java									
Nampu	J1	− 8.210442	110.904169	2.0	1.2	0.3	5.3	2.4	3
Klayar	J2	− 8.223617	110.947155	3.3	1.7	1.8	1.4	5.8	4
Blosok	J3	− 8.234227	110.965912	3.4	2.2	0.3	9.3	9.6	4
Pede-nombo	J4	− 8.241134	110.983327	1.8	1.4	0.3	5.3	2.4	5
Pidakan	J5	− 8.255659	111.238847	2.1	1.4	0.2	8.8	3.3	2
Papuma	J6	− 8.435089	113.551749	2.4	1.9	0.3	7.2	4.7	4
Bali									
Pandawa	B1	− 8.843602	115.189514	2.6	1.8	0.3	7.3	4.6	3
Lombok									
Are Guling	L1	− 8.913288	116.243961	2.5	1.3	0.3	6.3	3.2	4
Putinyale	L3	− 8.909685	116.298494	2.2	1.8	0.4	5.0	4	4
Payung	L4	− 8.917953	116.329526	3.6	2.8	0.6	5.3	10.3	4
Kura-Kura	L5	− 8.919369	116.441725	3.4	2.3	0.3	9.5	7.9	5
Sumba									
Maloba	S1	− 9.777156	119.651881	2.5	1.8	0.5	4.3	3.9	5
Kisar									
SW coast	K1	− 8.050024	127.138544	1.8	1.2	0.6	2.5	2.2	8
SW coast	K2	− 8.089577	127.146065						20
SW coast	K3	− 8.097237	127.145059						19
Leti	Lt1	− 8.213141	127.60159	3.2	1.6	0.6	4.0	5.1	4
Nailaka	Bn1	− 4.535583	129.696464	2.7	1.5	0.4	5.3	4.1	3

A—Flatness index $(Fb) = (a + b)/2c$

round boulder, whereas higher values are tabular rock slabs like those found in most IBD (Table 1).

Debates about the origins of IBD, whether from tsunami or storm waves, are blurred by lack of direct observations of how they form (e.g., Engel and May 2012; Medina et al. 2011; Shah-Hosseini et al. 2011; Kennedy et al 2021). Indonesia is optimal for exploring mechanisms of IBD formation because it is regularly impacted by observed tsunami and storm waves. Coastal boulder deposits in Indonesia are documented from tsunamis in 1883 and 2004, and a new discovery described in this paper from the 1994 tsunami in east Java (see below). The influence of storm waves on coastal boulder deposits is poorly constrained, which we address in this paper from 3 years of observations of one prominent IBD in East Java.

1.3 High energy storms in Indonesia?

The low rotational power of the Coriolis effect in Indonesia, which is $< 10°$ latitude, protects it from most cyclones. The rare cyclones develop spin south away from Indonesia toward higher latitudes. Less than one percent of all the tropical cyclones from 1907 to

2017 in the Australian region crossed into Indonesian territory (Mulyana 2018). In 2017, two category 1 tropical cyclones originated off the coast of Java but did not make landfall (Windupranata 2019; Avia 2020). Sea wave heights from the storms increased from a 0.5 m normal wave height to an average of 2 m, with some waves locally reaching 3.2 m. However, much of the energy from these storms dissipates as the waves crash into the fringing reef at the edge of the shallow sub-tidal platform offshore. Notably, these storms did not form IBD. The only coastal boulder deposits documented from a Sunda Arc subduction zone earthquake are associated with the 2004 Indian Ocean Tsunami (Etienne et al. 2011; Szczucinski 2012).

1.4 History of tsunamigenic earthquakes along the Java trench

Some of the most densely populated coastal areas in Indonesia are adjacent to the Java Trench. Historical records provide fuzzy data for only a few tsunamis (Wichmann 1918, 1922) that happened near Pacitan (Fig. 2) in 1840 and 1856, both of which were associated with earthquakes with shaking intensities of MMI of VII (Harris and Major 2016). The 1840 event shook for around two minutes. The lack of historical accounts that hint of mega-thrust earthquakes along the Java Trench may also be a function of lack of Dutch colonies along the coast or the slow-rupture style of earthquakes in the region. Early eighteenth-century Dutch maps show the southern coast as" Parte Incognita" with virtually no Dutch settlements. Slow-rupture earthquakes (Bilek and Lay 2002), which are common on the Java Trench, may also account for lacking historical accounts of strong shaking.

Only two instrumental earthquakes > Mw 7.0 have happened along the subduction interface of the Java Trench in the past century (Figs. 1, 2). These struck on 03/06/1994 (Mw 7.6 from Tsuji et al. 1995a, or Mw 7.9 from Hébert et al. 2012; Xia et al. 2021) and 17/07/2006 (M7.8 from Moore et al. 2011). Neither earthquake was felt by most coastal inhabitants (MMI < IV) because they were slow slip, "tsunami earthquakes" (Synolakis et al. 1995; Polet and Thio 2003; Fritz et al. 2007; Bilek and Engdahl 2007). Tsunami earthquakes produce uncommonly large waves relative to their recorded magnitudes (Tsuboi 2000) and generate surface seismic waves with longer periods and slower velocities than typical subduction earthquakes. Tsunamis from these two earthquakes had average wave heights of 5–7 m with maximum heights of up to 21 m in 2006 and 14 m in 1994 (Fig. 2). There was only 30 min between the nearly imperceptible shaking and the arrival of the tsunamis. Both tsunamis also reached the NW coast of Australia with run up heights of around 4 m (Nott 2000; Prendergast and Brown 2012).

1.5 Paleo-tsunami evidence in the eastern Sunda Arc

Although historical records provide evidence of at least four earthquake-generated tsunamis hitting Java's southern coast, much of the corresponding geologic footprint of tsunamis is not well preserved. For example, evidence of Krakatoa's massive 1883 tsunami, which produced 37 m high waves and killed over 36,000 people in West Java, is difficult to locate due to bioturbation, mass wasting, fish farming, resorts, industry, and agriculture (Paris et al. 2014). Java is the most densely populated, large island on Earth. Parts of the island that are not built upon are cultivated resulting in few undisturbed coastal areas.

Java is also one of the world's wettest islands located along a convergent plate boundary. Because of this, trenching efforts to prospect for candidate tsunami sand deposits are hampered by high levels of bioturbation and groundwater saturation. From our observations,

most of the deposits from the 1994 and 2006 tsunamis are not preserved. These factors make it possible that lack of candidate tsunami sand deposits is unrelated to tsunami size or recurrence. Recent attempts to locate paleotsunami sand sheets in swales of coastal plains of southern Java have yielded some success (Rizal et al. 2017; Sulaeman 2018). However, unequivocal diagnostic depositional features of tsunami sand layers are difficult to distinguish from storm deposits (Dawson and Shi 2000; Goff et al. 2001; Scheffers and Kelletat 2003; Morton et al. 2007; Switzer and Jones 2008; Bourgeois et al. 2009; Chagué-Goff et al. 2011).

The recognition of coastal boulder deposits along shorelines impacted by high-energy events, which include tsunamis, may provide a durable alternative to ephemeral tsunami sand deposits for recognizing the extent of tsunami impacted coastlines (e.g., Nott 2000; Nandasena et al. 2011a). For this study, we identified several sites along the southern coasts of the eastern Sunda Arc and Banda Arc where Google Earth images and attached photographs hinted that IBD exist. Ground surveys discovered at least 17 different IBD sites (Figs. 1, 2). The most likely processes that form these deposits are storm waves, tsunamis, or a combination between the two. The challenge is to unequivocally differentiate between these two different mechanisms that may produce the same landforms (Nott 2003; Switzer and Burston 2019; Cox et al. 2020). Tracking boulder movement before and after storms can establish limits for the influence of storm waves in forming or shaping IBD (Oak 1984; Lorang 2000; Goto et al. 2007; Goto et al. 2009b; Benner et al. 2010; Goto et al. 2010a; Goto et al. 2010b; Etienne and Paris 2010; Goto et al. 2011; Schneider et al. 2019). Age analysis of material buried by IBD is also key for determining if ages cluster or are scattered.

In this paper we document the characteristics of IBD adjacent to the Java Trench and use movements and age analysis of boulders to test possible mechanisms for the emplacement and modification of IBD.

2 Methods

2.1 Beachrock slab measurements

We conducted both aerial and ground surveys to measure the size and shape of individual beachrock slabs staked in the IBD. Only the length and width (a and b axes) of the rock slabs are measurable from aerial surveys, while the thickness (c-axis) of the slabs is measured on the beach itself. Measurements on the ground included > 30 random, 3-axis beachrock slab measurements at each site. We also measured the 5 largest slabs at each site and report the mean of these dimensions in Table 1. Measurements were also taken of the strike of the boulders to compare with the strike of the beaches (Meservy 2017).

2.2 Multi-year sUAS surveys of boulder movement

We surveyed boulder positions at Pedenombo beach during four separate sUAS (small Uncrewed Aerial System) survey missions flown between 2016 and 2019. The first pre- and post-storm measurements were taken on 30–31/07/2016 and 2/8/2016, which was immediately before and after a 4.2 m swell that struck the beach during $a + 2.5$ m spring high tide (Surfline.com). The third set of sUAS images were taken on 12/07/2017 after an epoch

of 342 days. The fourth set was taken 20/06/2019 after an epoch of 708 days. During this nearly 2-year period the beach was impacted by waves from two offshore tropical cyclones.

We documented boulder positions and movements using very well georeferenced, very high-resolution (0.5–1.0 cm) digital surface models (DSMs) and orthoimagery (Bunds et al., in press). The DSMs and orthoimages were produced with structure-from-motion (SfM) processing in Agisoft Photoscan and Metashape of optical imagery (i.e., photographs) collected with sUAS. sUAS used are DJI Phantom 2 customized to carry a 24 MPixel Sony A5100 camera (2016 data), DJI Phantom 4 Pro sUAS equipped with a 20 MPixel camera (2017), and a DJI Mavic Pro with a 12.3 MPixel camera (2019). The datasets were georeferenced using temporary ground control points (GCPs; 1.5 m iron-cross tarps) surveyed using post-processed kinetic differential global navigation satellite system methods (dGNSS). To improve surveying precision, we utilized local reference stations for which positions were determined using Jet Propulsion Laboratory's Automatic Precise Positioning Service. Co-registration of data sets collected over a 3 year period at one site was further improved using permanent, natural features present throughout the 3-year experiment. Vertical differencing of DSMs from different times was used to detect movement of boulders. Vertical differencing was performed using raster math tools in ArcMap.

2.3 Radiocarbon dating

Radiocarbon age analyses were also conducted on several coral boulders imbricated with beachrock. Care was taken to sample only the most deeply buried coral boulders that most likely reflect ages of IBD formation. Ages were determined by the Center for Applied Isotope Studies at the University of Georgia and were then calibrated using the online version of Calib 7.10 (Stuiver et al. 2019). Ages were calibrated (cal yr B.P.) to a 2 s (95% probability) error range, where zero age is AD 1950. The non-marine (charcoal and root sheath) sample ages were calibrated using the SHCal13 curve (Hogg et al. 2013), and the marine sample (coral and shells) ages were calibrated using the Marine13 calibration curve (Reimer et al. 2013). Reservoir correction was determined by averaging ΔR data from nearby locations in northwestern Australia and western Java (Southon et al. 2002; O'Connor et al. 2010, and Bowman 1985). Locations were chosen with consideration for proximity and ocean circulation. The value used for calibration was $\Delta R = 53 \pm 16$, with a lab error multiplier of 1.

2.4 Tsunami hazards models

Numerical models of potential inundation of a mega-thrust earthquake-generated tsunami along the Java Trench were constructed using ComMIT (Titov et al. 2011). ComMIT is an interface developed for NCTR (NOAA's Center of Tsunami Research) that utilizes a "Method of splitting tsunamis" (MOST). This program employs the shallow water equations for custom made fault plane solutions to model tsunamigenic earthquakes. The process is broken up into three steps/grids with each grid containing progressively higher resolution bathymetry and topography. These three steps include earthquake, transoceanic propagation, and inundation of dry land. Bathymetry is from the ETOPO1 1 arc-minute gridded global relief model produced by the NOAA National Geophysical Data Center and has been interpolated from 60 to 3 arc seconds. However, higher-resolution bathymetry could improve the model but it has been released by the Indonesian government.

Topography is from the CGIAR SRTM 90 m version 4 digital elevation model produced by the CGIAR Consortium for Spatial Information.

Population within the inundation zone is calculated using two data sources: "World Pop" projected 2020 census distribution (www.worldpop.org.uk) and the 2015 "European Commission, Joint Research Centre" (JRC) census distribution (data.europa.eu). Through ArcMap GIS tools, data were clipped from inundated areas, and the sums were analyzed from both data sources.

3 Results

3.1 IBD in Java

We discovered 7 IBD sites in Java (Fig. 2, Table 1). There are likely others either buried in sand or in parts of the coast we could not access. Most of the IBD form where the coast is eroding and beachrock is exposed in the intertidal zone. The most significant discovery was at Papuma (site J6, Fig. 2), a beach impacted by a tsunami from the 1994 7.9 Mw earthquake in east Java (Figs. 1, 2). Although no tsunami height measurements were made at Papuma during post-tsunami surveys, nearby beaches recorded maximum tsunami heights from 11 to 14 m (Synolakis et al. 1995; Tsuji et al. 1995a, b). Eyewitness accounts from residents and fishermen claim that the IBD at Papuma (Fig. 4a), and another site to the east at Pasir Putih (site J7), formed during the tsunami. Although the IBD were not mentioned during post-tsunami surveys (Maramai and Tinti 1997; Synolakis et al. 1995; Tsuji et al. 1995b) residents who witnessed the tsunami independently provided first-hand accounts of changes to the coastline that occurred including the formation of the IBD.

Papuma beach consists of outcrops of beachrock in the intertidal zone with layers that differ in resistance to erosion (Fig. 4). The outcrops show evidence of plucking of beachrock slabs from the intertidal zone, with pluck marks that match the size and shape of nearby detached slabs (Fig. 4). The minimum distance between sites of beachrock excavation and the IBD is around 25 m up a beach slope of 5°. At the base of the IBD the slope steepens abruptly to as much as 10°–18° (Fig. 4). Individual boulders in the Papuma IBD have consistent average strike directions within 6° of the strike of the shoreline (Meservy 2017). After the tsunami, residents observed that some rock slabs were found on the beach road and further inland of the platform backstop.

Near Papuma is Pasir Putih, which translates to "White Sand Beach." Eyewitness accounts claim that the 1994 tsunami removed all the white sand from the beach and transformed it into one entirely covered by small (<0.6 m^2), subrounded imbricated boulders and cobbles of volcanic rock that spill several meters over the platform backstop into the forest. It is not known if the sand covering boulders were removed and the boulders were transported from the intertidal zone to the supratidal zone, or if the boulders were offshore and were transported from the subtidal zone to the supratidal zone. Either way the tsunami deposit formed from what boulders were available, which did not include exposed beachrock. This pattern of no IBD where there is little to no beachrock is nearly ubiquitous.

Further west along the southern Java coast in the Pacitan region, we discovered five additional IBD sites (Fig. 4). Most of the beaches there and at most other sites have a wide, flat platform that extends 150–200 m seaward from the toe of the beach to the edge of barrier reef. The platforms are easily traversed during low tide because the large waves at these locations break offshore against the fringing reef. Large blocks of broken coral litter

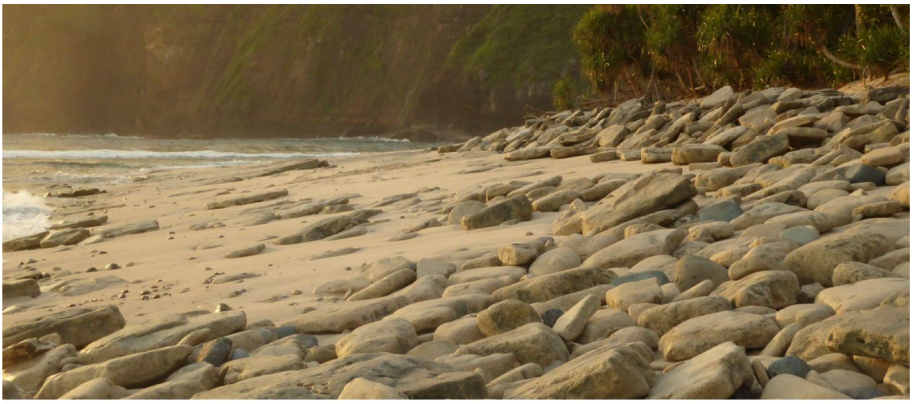

a.

b.

Fig. 4 IBD along the southern coastlines of eastern Sunda Arc islands of Java and Lombok. **a** Looking west at Pantai Papuma (site J6, Fig. 2), which was observed to form during the 1994 East Java earthquake-generated tsunami. Beachrock slabs in foreground have an average *a*-axis of 1.7 m. Notice the uniformity of imbricated beachrock slab composition, shape, and size. Deposit is stacked against landward edge of platform (see Fig. 3). **b** Pantai Pedenombo (site J4, Fig. 2) looking east. IBD forms landward of heavily solution weathered limestone ridge of the supratidal platform. Some beachrock and limestone slabs are found landward of the backstop on the forested coastal plain. See black and white aerial survey ground tarps, which are 1.5 m wide, for scale. **c** Detail of '*b*' looking west. Note how IBD have different amounts of weathering and smoothness. Deposit is littered with small (< 0.5 m *a*-axis), rounded, and circular boulders we observed being deposited by wind waves (see Fig. 3). Digital surface models of Pedenombo were constructed and compared to quantify storm wave influences over a 3-year period (see below). **d** Aerial image of Pantai Kura-Kura (site L4, Fig. 2) oriented east toward top. Note excavation scarps, and large, detached beachrock slabs that have not been added to the IBD yet. **e** Detail of **d** taken from western-most ground aerial control target showing large beachrock slabs at toe of IBD

c.

e.

Fig. 4 (continued)

the seaward edge of the platform, some of which have moved shoreward (Fig. 5). During storms the waves make it to the beach and cause erosion of the beachrock and cliffs.

According to Scheffers (2008) a shallow-water platform setting makes it difficult for wind waves to move boulders and rock slabs due to loss of energy not only when the waves break at the fringing reef edge, but also as they travel across the width of the shallow platform. The boulders at each site, and source areas for the boulders, are mostly beachrock like

d.

Fig. 4 (continued)

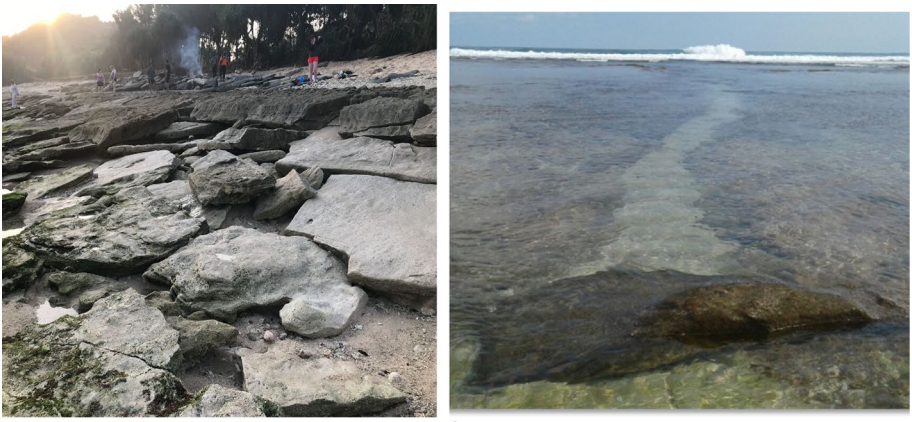

a. b.

Fig. 5 Typical coastal setting for the areas with IBD. **a** Beachrock slab excavation zone at Pantai Blosok (site J3). Excavation geometries have seaward dipping fault ramps and flats (see Fig. 3) where layered slabs were dislodged and transported landward against gravity. This excavation zone is typical of each IBD we discovered. Waves at Pantai Blosok normally break > 200 m offshore and are said by locals to never pass beyond the mangrove trees just landward of the boulders even during high wave events. **b** Looking south at wave cut platform offshore of Pantai Blosok with waves breaking on the seaward platform edge. In the foreground is a coral boulder (2 × 1 × 0.4 m) likely dislodged from platform edge

what we observe at Papuma (Fig. 4). Some beaches have slabs of limestone from nearby bedrock outcrops and coral mixed in with the IBD. Well exposed areas of beachrock excavation show ramp-flat excavation geometries like those in imbricate thrust sheets (Figs. 3, 5a). Most exposed areas of beachrock in the intertidal zone are adjacent to IBD.

The IBD at Pidikan is unique in that it consists of large, detached slabs of beachrock in the intertidal zone versus the supratidal zone where the other IBD stack up against the platform edge. This feature demonstrates how wave erosion can influence the formation of IBD by providing broken slabs of beachrock that have not yet been transported to the supratidal zone.

3.2 IBD east of Java

East of Java, IBD are found along the southern coastlines of Bali, Lombok, and Sumba of the Lesser Sunda Islands, and along coastlines of the Banda Arc Islands of Kisar, Leti and Nailaka (Fig. 1). The Lesser Sunda Islands face the Java Trench while the Banda Arc Islands face the Timor and Tanimbar Troughs, which are influenced by continental subduction (e.g., Harris 2011). In SE Lombok IBD are up to 750 m long and 25 m wide at Kura-Kura Beach (site L5, Fig. 2). Similar characteristics are found in these deposits as documented from the known tsunami deposit in Papuma.

3.3 Composition of IBD

The IBD we discovered mostly consist of slabs of carbonate-cemented sand and gravel of both clastic and biogenic origin (Fig. 6), which is characteristic of beachrock in general (e.g., Russell 1963; Bricker 1971; Milliman 1974; Vieira et al. 2007). Most of the IBD

Fig. 6 Beachrock consisting of carbonate-cemented clastic and bioclastic material

sites in the eastern Sunda Arc are near carbonate bedrock. Although beachrock is a common feature of coastlines globally, ridges of stacked or imbricated beachrock are rare.

Compositional exceptions to IBD are accumulations of coastal boulders sourced from wave-cut cliffs. These varying-shaped boulders are also imbricated by high-energy events (Fig. 7). Imbricated boulders not including beachrock are found at Nampu (site J1) and Klayar (site J2) in Java and Payung (L1) in Lombok (Fig. 2).

3.4 Size and orientation of IBD

Evidence of rapid undercutting and recent bedrock cliff failure and retreat is visible throughout much of southern coastlines of Java, Bali, Lombok, and the Lesser Sunda Islands. Typically, when a coastal cliff collapses, or a landslide occurs near the coast, rocks from onshore are initially distributed randomly along the coastal bench. Large waves can break up some of these boulders and stack them in with beachrock slabs (Fig. 7).

Fig. 7 Looking NW at large (~75 metric ton) imbricate boulder of volcanic rock in the intertidal zone at Payung, Lombok

In contrast, beachrock from the intertidal zone stacks up in a different way to produce IBD. In situ beach rock is constantly being attacked by storm waves causing differential erosion of some layers that introduce instabilities, such as overhangs that cause beachrock to break into allochthonous slabs like those found at Pidikan. Large waves transport most slabs from their source in the intertidal zone to near the maximum high tide mark to form IBD. Nearly all the stacked slabs of IBD are platy with average long a-axes of 2.8 m, intermediate axes (*b*-axis) of 1.8 m and thicknesses (*c*-axis) of 40 cm (Table 1). Volumes of the largest boulders are 3–4 m^3. In general, the largest rock slabs are around the same size, with exceptions found at sites J4 and L4 (Table 1).

Most IBD have a preferred strike orientation of the a-b plane that is sub-parallel to the strike of the shoreline within 2°–10° (Meservy 2017). All the beach rock slab accumulations have similar, right-skewed distributions with between 0.5 and 1.0 m^3 in volume. The degree to which this size limit is a function of wave height or speed, or from the size of the boulders available, or a mix of all three factors is unknown (Benner et al 2010). Other studies demonstrate how boulder sizes do not correlate well with known wave speeds that deposited them (Etienne et al. 2011). More important are the sizes of the boulders available for the wave to entrain (Scheffers 2021). Nott (2003) notes that during the 1998 Sissano tsunami in Papua New Guinea a concrete slab with *a*- *b*- and *c*-axes of 3.15, 1.22 and 0.23, respectively, moved 400 m inland from tsunami flow depths of 5 m. This depth is less than those inferred for Papuma.

3.5 sUAS images of storm wave-induced boulder movement

To track possible boulder movement during relatively large storms in the eastern Sunda Arc, we constructed sUAS-assisted digital surface models (DSMs) with a high degree of boulder registration (see Methods) during a 3-year period at Pedenombo beach (Figs. 8, 9). This beach consists of 3 platforms, the lowest of which is the current wave

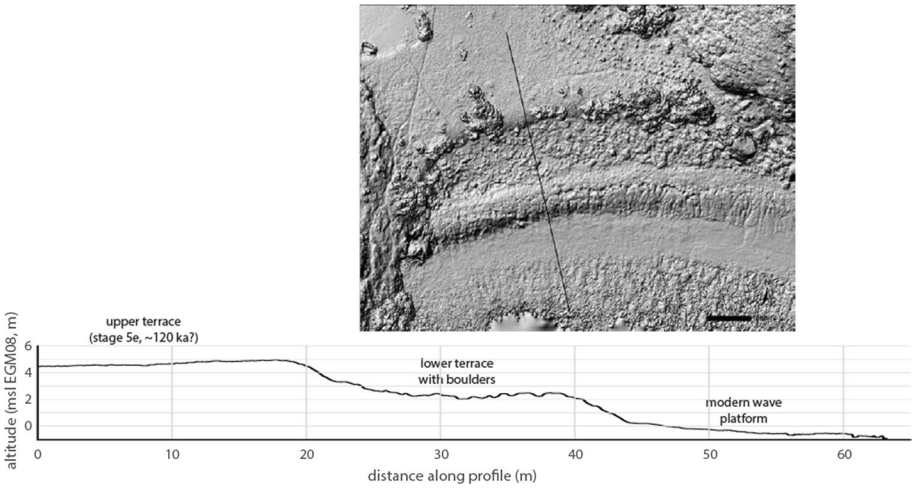

Fig. 8 Shaded relief image and profile of Pedenombo beach showing its three different wavecut platforms. IBD fill the area between the upper and lower terraces. Black line is position of profile. Note some boulders decorate the highest terrace at around 5 m MHW

(a)

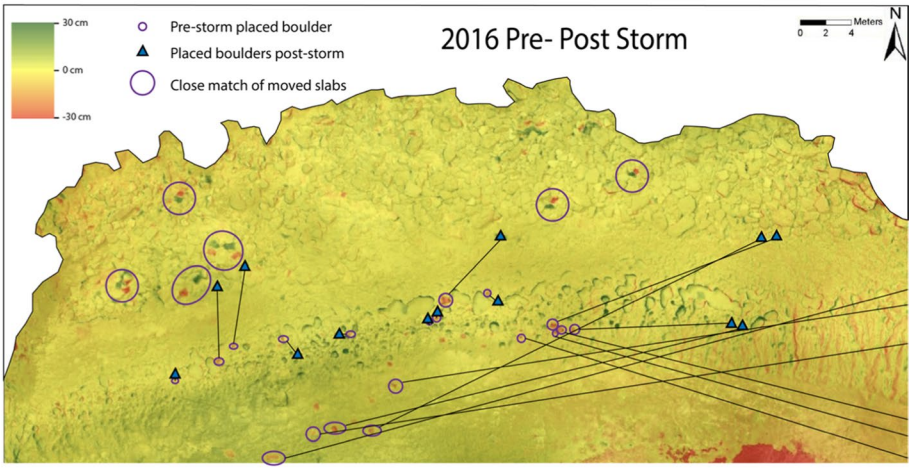

(b)

Fig. 9 **a**–**d** sUAS generated DSM overlays taken at 4 different times over a 3-year period at Pedenombo (site J4). Red signifies negative change in elevation of < -0.3 m. Green shows an elevation increase of < + 0.3 m. The outer rim of the beach shown in (**a**) is cropped in this and other images. Solution weathered pockets eroded into bare-rock platform 2 (Fig. 8) are useful for registering images. When measuring possible beachrock slab movement over longer periods of time, correlating slab excavation and addition marks is difficult due to deposition and removal of storm wave transported sand, gravel, and cobbles. Black and white ground tarps for aerial surveying are 1.5 m in length

cut terrace forming the intertidal zone. The next higher platform is 3 m above sea level and likely represents a storm wave terrace, which hosts the IBD that stack up against the shoreward edge of platform 3. Platform 3 is not dated but is likely an uplifted Holocene coral terrace or a slightly subsided 5e sea level high-stand terrace based on its elevation.

Image (a) is an orthophoto documenting the initial positions of IBD slabs 1 day before an uncommon storm wave event (Fig. 9a). Additionally, 21 limestone boulders < 0.4 m in diameter were marked, manually placed, and surveyed seaward of the IBD. See small open circles in Fig. 9b for original positions of hand placed boulders.

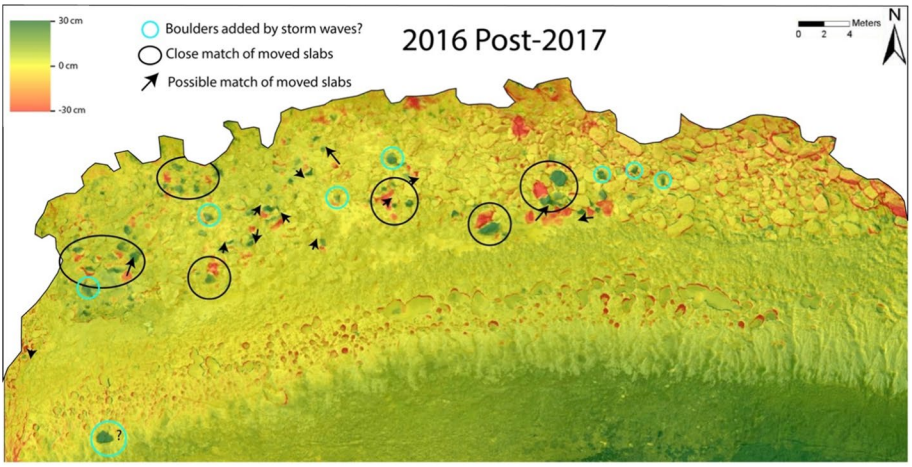

(c)

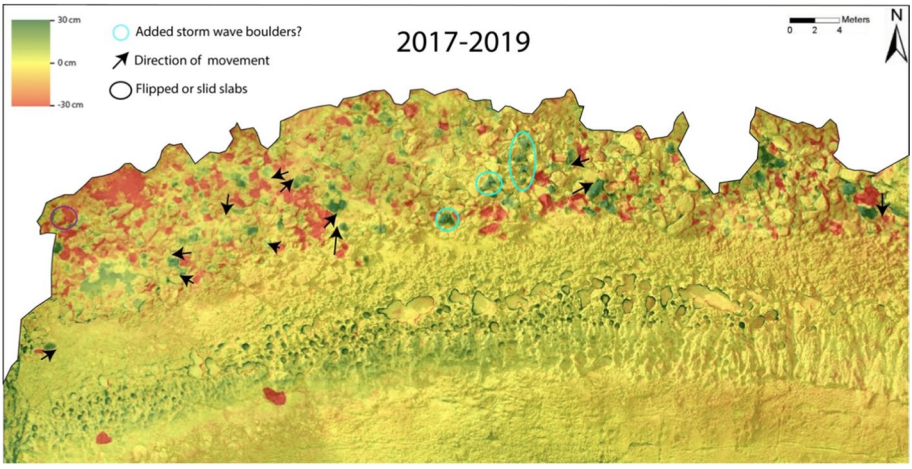

(d)

Fig. 9 (continued)

Image (b) is an overlay of DSMs from before and after the 6.7 m high wave event on 30–31/07/2016 (Fig. 9b). The image documents the initial and final positions of manually placed boulders and pre-existing beachrock slabs of the IBD (Fig. 11b). After the storm, we located all but two of the boulders and resurveyed their positions. Green circles show pre- and red triangles show post-storm locations. Lines on the image connect initial and final boulder positions and reveal that all manually placed boulders moved, if only 10 cm. Most boulders moved laterally along the shoreline, even off the image from 2 to 45 m. Five placed boulders were added to the front of the IBD, but none moved onto the IBD. At least 8 pre-existing beachrock slabs of the IBD moved < 2 m as indicated by the proximity of slab excavation and addition marks. The mirror image of some of these marks indicate slabs flipping about their *a*-axes.

Image (c) is an elevation difference map made from the post-storm 2016 and 2017 sUAS surveys. During this time, waves from 2.2 to 2.6 m were recorded on 23/06/2017 (Avia

2020). At least 19 IBD slabs moved <2 m based on matching of green and nearby red shapes (Fig. 9c). The mirror image of some of these shapes indicates slab flipping about the *a*-axis as in Fig. 9b. At least 8 other slabs circled in green have ambiguous sources. These slabs may have been added to the IBD by storm waves (not likely based on other observations) or their original position is eroded or filled in by storm deposited sand, gravel, and cobbles. Changes in sand volume are detected at ten localized zones on the beach with an average volume change of approximately 65 m^2.

Image (d) is an elevation difference map made by subtracting the 2017 DSM from the 2019 DSM, and it records the effects of some of the most energetic waves over the most time (two offshore tropical cyclones). During this time, overlapping category 1 cyclones Cempaka and Dahlia brushed by Java increasing wave heights from 1.8 to 3.2 m (Widupranata 2019; Avia 2020). Cempaka nearly made landfall in the Pedenombo beach area, affected 13 coastal communities near Pacitan. In total there were 41 deaths, 20,000 people evacuated, and around US$83.6 million in damages (Badan Nasional Penanggulangan Bencana). Although the final overlay is messy due to clastic sediment redistribution, it reveals that around 113 individual beachrock slabs moved slightly or flipped of the approximately 1220 slabs in the IBD. One boulder in the lower left corner of image (c) disappears in image (d).

It is important to acknowledge the possible cumulative effect of wave action flipping and transporting beachrock slabs within the IBD. If around 113 beachrock slabs are displaced to some degree, then over the century-long time frames of possible boulder ages tens of thousands of boulders have shifted. However, *there is no conclusive evidence of boulder addition or removal.* sUAS-based post-tsunami surveys of the 2004 Indian Ocean Tsunami also found that no boulders were added to or removed from the tsunami formed IBD by monsoonal storms (Etienne et al. 2011). Yet, it is important to recognize the key role storm waves plays in eroding beachrock in the intertidal zone into loosened and detached slabs that can be transported later by tsunami waves. These results may reveal the limits for Indonesian storm waves to move boulders and strongly support an interpretation that the IBD are preprocessed by storm waves but primarily moved and stacked by tsunamis.

3.6 Radiocarbon analyses

Another way to test the relative contribution of storm versus tsunami waves in forming IBD is age analysis of coral boulders interlayered with the beachrock slabs. Dating IBD is problematic due to the likelihood of mixing offshore siliciclastic and bioclastic material of various ages (e.g., Mastronuzzi and Sans`o, 2000; Ishizawa et al. 2020). Age clustering may differ depending on whether coral boulders were emplaced by storms or tsunamis. Tsunami ages may cluster around the time of known historical or paleo-tsunami event, whereas storm wave deposits could have a much broader age distribution since coral boulders could be added more regularly. To try to avoid mixing of coral and shell material deposited by storms onto the IBD with material deposited at the same time as the IBD, we were very selective in the coral boulders we sampled to make sure it was highly unlikely that they could not have been wedged into the IBD later. Most of the coral boulders were smaller than the beachrock slabs but are buried beneath them.

Our reconnaissance age analysis of several coral boulders and shell material yielded reliable ages at 5 sites (Table 2). Although there is some scatter, most ages correspond closely with known historical tsunamis (Harris and Major 2016) and candidate paleo-tsunamis in the eastern Sunda Arc (Sulaeman 2018). Only six tsunamis affecting the south

Table 2 Radiocarbon chronology of shells and coral boulders within five IBD in Java

Location	Sample type	Calibrate calendar age	95% confidence	Possible event
Binuangeun West Java	Shell	1053 AD	990—1153 AD	1200–800 AD Java Trench*
	Shell	991 AD	908—1050 AD	1200–800 AD Java Trench*
	Coral boulder	989 AD	907—1049 AD	1200–800 AD Java Trench*
	Shell	905 AD	806—994 AD	1200–800 AD Java Trench*
	Coral boulder	663 AD	596—724 AD	?
Blosok-C Site J3	Coral boulder	1861 AD	1810–1880 AD	1859 AD Pacitan
Blosok-B Site J3	Coral boulder	1692 AD	1640–1720 AD	1699 AD Java
Blosok-A Site J3	Coral boulder	551 AD	500–580 AD	?
Pidakan Site J5	Coral boulder	1474 AD	1440–1510 AD	1400–1600 AD Java Trench*
Pedenombo Site J4	Shell on boulder	1177 AD	1080–1220 AD	1200–800 AD Java Trench*
Kisar 1** Site K1	Coral boulder	1903 AD	1898–1908 AD***	1896 AD Timor
Kisar 2** Site K2	Coral boulder	1904 AD	1897–1909 AD***	1896 AD Timor

*Sulaeman (2018), **Boulder deposit on coral terrace, ***Major et al. (2013)

coasts of eastern Sunda Arc islands are recorded in historical accounts dating back to 1584. This lack of possible events reduces the likelihood of coral boulder ages randomly coinciding with known and inferred tsunamis by chance (Table 2). For example, the 1861 AD age of coral boulders in IBD near Pacitan is concordant with the 1859 Pacitan tsunami (Harris and Major 2016). The 1692 age of another boulder coincides with one of the largest earthquakes to strike Java documented in historical accounts. This event was felt widely throughout the region with a maximum MMI of X, had at least 13 months of aftershocks, and triggered a tsunami of unknown extent (Harris and Major 2016). The 1474 AD age correlates with a 400–600 years BP OSL age of a candidate tsunami sand deposit at 1 m depth in Bali (Sulaeman 2018). Similar high-energy sands with marine debris occur onshore at around the same depth throughout the southern coastal plains of the Lesser Sunda Islands (Sulaeman 2018).

We also found relatively young boulders deposited up to 20 m above sea level on the 125 ka uplifted coral terrace in Kisar (Major et al. 2013). These ages are concordant with the 1896 earthquake and tsunami in Timor, which is the only major earthquake from the Timor region found in over 400 years of historical records (Harris and Major 2016).

The wide spectrum of ages for the imbricate coral boulders we sampled across the widely spread beaches may result from many factors, which is common for coastal boulder accumulations (e.g., Vousdoukas et al. 2007). The age ranges are consistent with IBDs amassing over a series of events (Nott 1997, 2004). Notwithstanding these issues, we point out that it is highly unlikely that most boulder ages cluster with the limited number of

events reported in historical records and the two proposed paleo-tsunami events in region. In fact, only two ages that do not correlate are those of 500–700 AD (Table 2). If these boulder ages correspond to a tsunami, they are consistent with the pattern of century-long gaps of time between events, which may correspond to the amount of stress loading required for mega-thrust earthquakes to produce tsunamis that form IBD.

4 Discussion

4.1 Storm or tsunami origin for IBD

Although huge individual boulders and even boulder ridges may have been emplaced and modified by wind waves (e.g., Goto et al. 2011; Cox et al. 2019), the construction of well-organized and imbricated beachrock slabs are not documented from even the largest known cyclones (Mastronuzzi and Sans`o 2000; Noormets et al. 2004; Nott 2004; Saintilan and Rogers 2005; Scheffers et al. 2005; Suanez et al. 2009; Switzer and Burston 2020; Scheffers and Kinis 2014). Perhaps this pattern is a function of the long duration and large amounts of water associated with tsunamis that can have orders of magnitude more transport energy than the largest storm waves (Scheffers 2021).

Our literature search found little evidence of IBD *like those we observe in Indonesia* that formed from known cyclonic storms. If it is common to form IBD from cyclones, then they would be a common feature of coastlines where beachrock is exposed to cyclones worldwide (Ginsburg 1953; Lau et al. 2015). The stunning imbricated bedrock slab deposits on the shores of Lafkaniska and Murroogh Point in western Ireland are interpreted as a classic example of storm wave emplaced IBD due to lack of tectonic activity (Cox et al 2012, 2019, 2020). However, ages of the boulders reach back into the early to mid-Holocene when sea level was lower (Erdmann et al. 2015). These results indicate that most of the larger boulders have not moved for centuries to millennia. If storms primarily form IBD there would be multiple deposits associated with them in areas with beachrock that are battered regularly by cyclones, like NW Australia. Coral boulders caught up in storm-formed boulder deposit should have a wide range of ages. Infragravity deposits should have a wide range of ages as well with no detectable clustering between long hiatuses.

Other IBD interpreted as storm-emplaced in areas with little tectonic activity exist in the Bahamas (Raphael 1975) and Brazil (Cooper et al 2019). The IBD in the Bahamas example is not correlated with any single hurricane event, but many have struck the region. As for the IBD in Brazil, it is important because, like Indonesia, it is does not experience intense cyclonic storms as in the Bahamas. Tabular panels of beachrock in the Brazil example have similar characteristics to those we discovered in Indonesia. However, the slabs of beachrock are not stacked in the supratidal zone, but instead form in situ presumably due to wave erosion without transport upslope. Eroded slabs dip both landward and seaward because they likely slide off beachrock outcrops as wave-cut overhangs collapse. The erosional instabilities produce slabs up to 40 tons that are mostly autochthonous. Similar wave erosional processes of beachrock are found at Kura-Kura (Fig. 4d) and Pantai Pidikan during this investigation.

As revealed by DSM elevation difference maps, matching boulder movements at Pedenombo indicate that storm waves modify existing IBD by flipping and possibly sliding boulders short distances. At many beaches the most shoreward part of beachrock outcrops is undercut by wave action where the beachrock layers dip steeper than the beach

slope angle. The overhangs that result commonly have rounded boulders (< 0.5 diameter) wedged into them likely from backwash. The wedging effect exerts an upward force on the overhangs and in some cases cause them to split off. These examples document how storm and tsunami wave action combine forces to form and shape IBD.

Small (< 1.0 m^2) boulders we placed beachward of the IBD mostly moved eastward parallel to the longshore drift with some stopping at the toe of the IBD. Over the 3-year period that we tracked the IBD boulders, around > 10% detectably moved. Consistent with observations by others (Nott 2003; Scheffers and Kinis 2014), no boulders were excavated from beachrock outcrops and added to the IBD by storm waves. The storms that impacted the IBD during the 3-year epoch, which are the largest storms ever documented along the southern Sunda Arc coast (Windupranata et al., 2019), did not form IBD. Ages of coral boulders in IBD correspond to known historical, and inferred paleo-tsunami events that are separated by centuries. Ages from similar boulder deposits in Australia and the Sunda Arc also show 400–600-year age gaps.

Scheffers (2004) concludes that boulder deposits from tsunamis are more likely to form ordered imbricate stacks of beach boulders due to the length of time tsunami waves inundate versus the disarray of most boulders emplaced by storm waves. Again, this interpretation is consistent with the lack of documented boulder ridges in places impacted by gigantic storms, such as the NW coast of Australia (Nott 2000).

4.2 IBD and mega-thrust earthquakes

The discovery of several tsunami-related IBD along a 1200 km section of the south coastal regions of the eastern Sunda Arc (Sulaeman 2018), which are likely emplaced by tsunamis, indicates that this region is possibly as susceptible to recurring mega-thrust earthquakes and large tsunamis as the western Sunda Arc (Sumatra). Candidate paleo-tsunami sand deposits discovered throughout the eastern Sunda Arc also attest to at least two large, multi-island tsunamis at around 1000 and 1500 CE (Sulaeman 2018). These findings are consistent with ages for some of the shells and coral boulders incorporated into the IBD of the Sunda Arc and NW Australia.

Recent studies of seismic coupling (Hanifa et al 2014; Koulali et al. (2017); Gunawan and Widiyantoro 2019) indicate that two large sections of the Java Trench are accumulating elastic strain and are not in a state of creep, as suggested by others (e.g., Newcomb and McCann 1987). Many of the IBD we discovered at other locations are like those at Papuma, although some sites have much larger boulders. The size of beachrock slabs may depend more on joint spacing, pre-tsunami storm wave processing, or fragmentation during transport (Oetjen et al. 2021).

4.3 NW Australia IBD from Java trench tsunamis?

IBD decorating the southern coastlines of multiple eastern Sunda Arc islands have similarities to those in NW Australia, such as the average size of the largest slabs, slab vs beach strike, composition, age, and clear excavations or dislodgements seaward from the IBD. Interpreting the processes involved in IBD formation is helped by a known tsunami emplaced IBD at Papuma. IBD and large boulders at elevations up to 20 m along the 2500 km of coastline of NW Australia document huge wave impacts before historical times (Nott and Bryant 2003; Goff and Chague-Goff 2014). Imbricated boulder ridges, like those we discovered are documented up to 6 m elevation. The largest boulder measured

in Australia IBD has an *a*-axis of 5 m, but the average boulder sizes are $a = 3.0$, $b = 2.1$, $c = 0.7$ m (Nott 2004). Shells at the back of the ridge have radiocarbon chronologies dating around the mid to late nineteenth century, a period of heavy seismicity near Pacitan (Harris and Major 2016). Other ages roughly align with those of pre-historic tsunamis, including centuries-long time gaps (Table 2).

Tsunamis that have impacted NW Australia during the last century were generated by the 1977 Sumba earthquake (Mw 8.3, Pradjoko et al 2015), and the 1994 (Mw 7.8) and 2006 (Mw 7.7) Java Trench earthquakes (Burbridge et al. 2009). Runup heights in NW Australia from the 1977 and 1994 tsunamis were around 4 m (Nott and Bryant 2003). The 1994 tsunami transported coral boulders and marine fauna over 1000 m inland. The 2006 tsunami, which was further north on the Java Trench, had a flow depth of 1–2 m, maximum runup of 8 m, and inundated around 100–200 m inland (Prendergast and Brown 2011). None of the tsunamis formed new or noticeably modified existing IBD.

The NW Australian IBD at Exmouth consist mostly of beachrock like those we discovered in the eastern Sunda Arc. The fact that the 1994 Java Trench tsunami formed an IBD along the Java coast, but not in Australia may indicate that the Australia deposits require larger tsunamis from mega-thrust earthquake events. According to the age analysis of the boulders in the Exmouth IBD, a tsunami of this scale happens over time intervals of 400–500 years (Nott 2004), which is consistent with IBD coral age distributions in the eastern Sunda Arc (Table 2). The age results from Australia and eastern Sunda Arc also argue strongly against IBD being formed by cyclones, which happen on a much more regular basis and have been checked, without success, for IBD.

To test the potential of cyclones forming the NW Australia IBD, Nott (2004) conducted pre- and post-cyclone visual surveys. One of the mega-storms was TC Vance, which is the most intense category 5 cyclone ever recorded to cross Australian shores. Surveys were also taken after 3 other category 5 cyclones. These surveys found no evidence of IBD development even in areas where abundant loose boulders were available in the intertidal zone. Nott (2004) also claims that existing IBD were not disturbed by the mega-storms and no new beachrock slabs were added or removed. It is possible that IBD from the Indonesian locations described in this paper and the ones at Exmouth, Australia may be emplaced by tsunamis from the same earthquakes with those of Australia only recording megathrust events on the Java Trench.

4.4 Tsunami hazard models and maps

If IBD in the eastern Sunda Arc and northern Australia record mega-thrust earthquake-caused tsunamis on the Java Trench, most of which have no historic precedent, then tsunami hazards risk assessments should consider the likelihood and impact of these events. To investigate this impact, we constructed tsunami models for two earthquake scenarios along the Java Trench, both of which could potentially form IBD simultaneously along the south coast of the eastern Sunda Arc islands and in NW Australia. We include estimates of the number of people currently inhabiting the areas of inundation in the models.

Model 1 is for an earthquake simulation that fills the seismic gap between the 1994 and 2006 subduction interface earthquakes on the Java trench south of Java (Figs. 1, 10). This gap could have ruptured to produce the 1859 and 1699 earthquakes and tsunamis noted in the Pacitan area (Harris and Major 2016). Rather than using a generic slip distribution model we substitute the slip distribution from the 2011 East Japan earthquake to make the model more viable. The subduction characteristics of the Japan

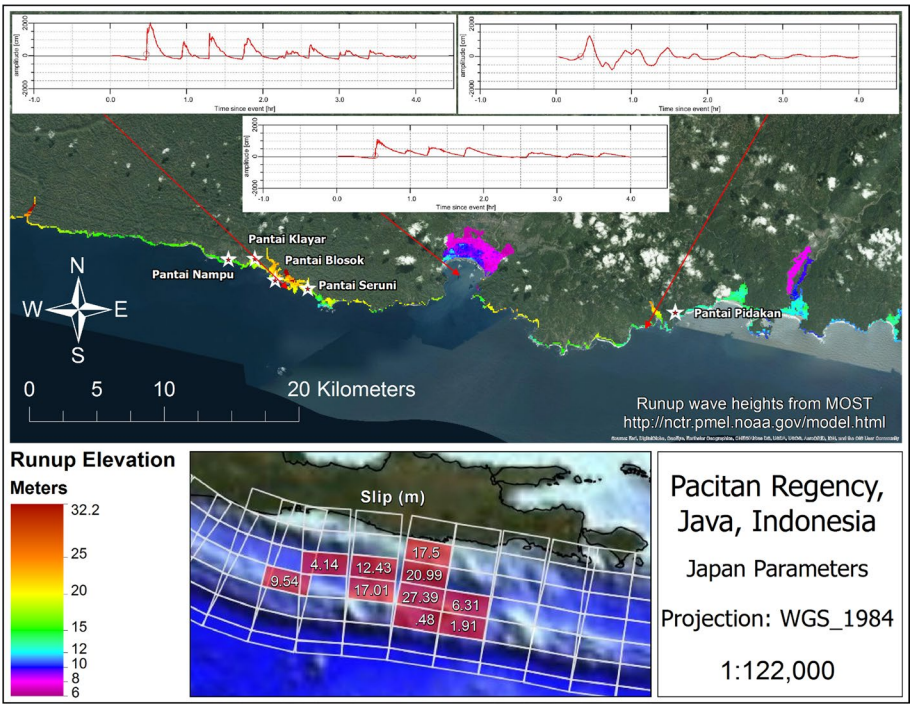

Fig. 10 Model 1 of an 8.4 Mw earthquake on the segment of the Java Trench between the locations of the 1994 and 2006 Java Trench earthquakes. The slip distribution along the fault is like that used in Titov et al. (2016) for the 2011 Tohoku earthquake. Red dots are the locations of simulated tidal gages that match with the red lines time series data. These data predict the arrival of a ~20 m wave 20–30 min after the initiation of the earthquake. Interestingly, the location of the IBD (stars) is where the model predicts the highest wave runup of 20–25 m

Trench near the Sendai region of Japan are very similar to those of the Java Trench. In both areas convergence rates are high and subduction of old oceanic crust with thin sedimentary cover and multiple seamounts parses the subduction zone into relatively small segments. The model shows the tsunami runup elevation of up to 25 m from a Mw 8.4 earthquake on the subduction interface near where most of the IBD in Java are found (Fig. 10). The inundation distance inland is limited here because the coastline is erosional with few coastal plains.

Model 2 (Fig. 11) is a worst-case scenario Mw = 9.0 mega-thrust earthquake that ruptures the seismic gap along the entire Java Trench. The amount of slip in this model is based on the sudden release of 28 m of elastic strain or tectonic loading that has already accumulated on the 1200 m length Java Trench during the past 478 years (Harris and Major 2016). Wave heights at Kura-Kura and other IBD sites in Lombok are estimated up to 35 m. More than 6 million people inhabit the inundation zone of the simulated tsunami. The transoceanic propagation of this event (Fig. 12) shows the highest open ocean waves striking the western most tip of Australia where most of the IBD reported from this region are observed (Nott 2000).

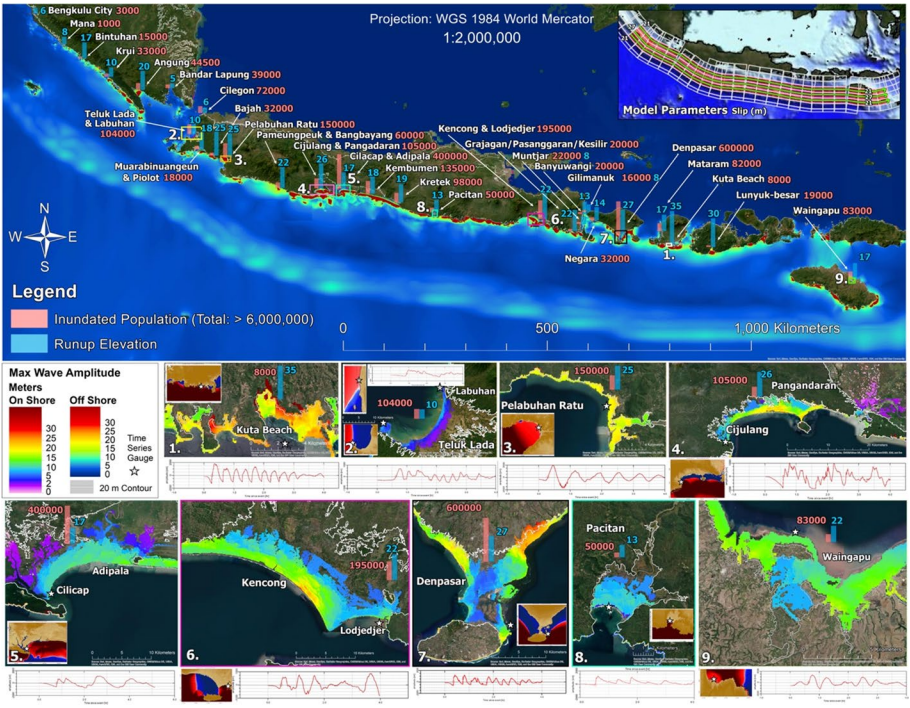

Fig. 11 Tsunami Model 2 of full Java Trench seismic gap rupture (from southern-most Sumatra to Sumba). Model slip distribution is shown in upper right. Top map shows inundation, runup (blue bar) and population estimates of cities in the inundation zone (red bar). Bottom—detailed maps of the most populated areas. Small inset map shows arrival of first wave offshore next to four-hour time series of wave arrivals. The gray line onshore is the 20 m elevation contour

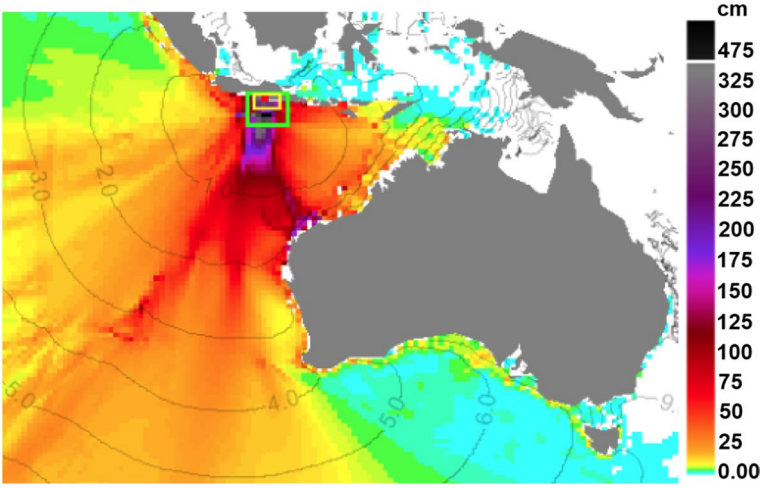

Fig. 12 Model 2 trans-oceanic wave height distribution showing tendrils of the highest waves (dark colors) focusing energy on the Exmouth, Australian region where IBD are observed

5 Conclusion

We claim that IBD discovered adjacent to the Java Trench in Indonesia are primarily deposited by tsunamis, based on direct observations of 1994 tsunami-formed IBD at Papuma, the occurrence of long imbrication ridges of large boulders only adjacent to areas where beachrock was plucked from intertidal zones, the concordance of coral boulder ages with paleo and historical tsunami events, and lack of evidence from multi-year sUAS surveys for storm-produced IBD (even during the largest storms known). It should also be noted that the processes that form IBD are not ubiquitous but, rather, require unique conditions, such as the formation of beachrock in the intertidal zone, storm wave processing of outcrops, and coastal geomorphology for the IBD to form and persist.

The existence of the IBD, especially in densely populated coastal areas as Java, Bali, and the Lesser Sunda Islands, is natural 'warning stones' of where tsunamis have likely inundated coastal areas in the past and as such must be incorporated into tsunami hazard risk reduction strategies. Tsunami models of a worst-case scenario Mw = 9.0 megathrust earthquake show that over 6 million people inhabit areas that would be inundated by such a tsunami. Cities along the southern coast of the eastern Sunda Arc islands and other parts of Indonesia (Banda Arc) that have not experienced a mega-thrust earthquake in over 400 years are at high risk of tsunami hazards.

Acknowledgements Funding for this research was generously provided through grants from Geoscientists Without Borders, which is affiliated with the Society of Exploration Geophysicists (SEG). Additional funds were provided by In Harm's Way non-profit organization (inharmswayhelp.com), Utah Valley University (UVU), and Brigham Young University (BYU). We thank Universitas Pembangunan Nasional (UPN Jogjakarta) who sponsors our research in Indonesia. We owe a special debt of gratitude to Eko Yulianto and Purna Putra from LIPI for collaboration in paleotsunami research in Indonesia. We express appreciation for logistic assistance from the BPBD and governor's offices of Pacitan, Mataram, Waingapu, Leti and Ambon. We are grateful for the logistical coordination help of Deborah Harris. We appreciate the many students from UPN, UVU and BYU, and both foreign and local volunteers who helped throughout the project.

Author contributions All authors contributed to the study conception, design, material preparation, data collection and analysis. The first draft of the manuscript was written by WM and all authors commented on previous versions of the manuscript. All authors read and approved the final manuscript.

Funding Funding for this research was generously provided through grants from Geoscientists Without Borders, which is affiliated with the Society of Exploration Geophysicists (SEG). Additional funds were provided by In Harm's Way non-profit organization (inharmswayhelp.com), Utah Valley University (UVU), and Brigham Young University (BYU).

Declarations

Conflict of interest The authors have no relevant financial or non-financial interests to disclose.

References

Avia L (2020) A comparative analysis of the wind and significant wave height on the extreme weather events (TC Cempaka and TC Dahlia) in the Southern Sea of Java, Indonesia. In: IOP conference series: earth and environmental science, IOP Publishing Vol 572, no 1

Benner R, Browne T, Brückner H, Kelletat D, Scheffers A (2010) Boulder transport by waves: progress in physical modelling. Zeitschrift für Geomorphologie 54(3):127–146

Bilek S, Engdahl E (2007) Rupture characterization and aftershock relocations for the 1994 and 2006 tsunami earthquakes in the Java subduction zone. Geophys Res Lett 34:20

Bilek S, Lay T (2002) Tsunami earthquakes possibly widespread manifestations of frictional conditional stability. Geophys Res Lett 29(14):1673. https://doi.org/10.1029/2002GL015215
Boulton S, Whitworth M (2018) Block and boulder accumulations on the southern coast of Crete (Greece): evidence for the 365 CE tsunami in the Eastern Mediterranean. Geol Soc Lond Spec Pub 456(1):105–125
Bourgeois J, Bernard E, Robinson A (2009) Geologic effects and records of tsunamis. The Sea 15:53–91
Bowman G (1985) Oceanic reservoir correction for marine radiocarbon dates from northwestern Australia. Aust Archaeol 20(1):58–67
Bricker O (1971) Introduction: meteoric-water cementation. In: Bricker O (ed) Carbonate cements. Johns Hopkins Press, Baltimore, p 121
Bunds MP, Uribe AT, Andreini JC, Smith S, Barret B, Horns D, Harris RA, Prasetyadi C, Yulianto E, Putra PS, (in press), High resolution topography of imbricate beach deposits, Indonesia, OpenTopography
Burbidge D, Cummins P, Mleczko R, Thio H (2009) A probabilistic tsunami hazard assessment for Western Australia. In: Cummins PR, Kong LS, Satake K (eds) Tsunami science four years after the 2004 Indian Ocean tsunami: Part I: modelling and hazard assessment. Springer, Berlin, pp 2059–88
Chagué-Goff C et al (2011) Expanding the proxy toolkit to help identify past events—lessons from the 2004 Indian Ocean Tsunami and the 2009 South Pacific Tsunami. Earth Sci Rev 107(1–2):107–122
Cooper JAG, Green AN, Vital H, Lima-Filho FP (2019) Geomorphology and clast assemblages of intertidal beachrock: implications for submerged shoreline preservation. Geomorphology 343:106–118
Cox R, Zentner DB, Kirchner BJ, Cook MS (2012) Boulder ridges on the Aran Islands (Ireland): recent movements caused by storm waves, not tsunamis. J Geol 120:249–272
Cox R, O'Boyle L, Cytrynbaum J (2019) Imbricated coastal boulder deposits are formed by storm waves, and can preserve a long-term storminess record. Sci Rep 9(1):1–12
Cox R, Ardhuin F, Dias F et al (2020) Systematic review shows that work done by storm waves can be misinterpreted as tsunami-related because commonly used hydrodynamic equations are flawed. Front Mar Sci 7:4
Dawson A, Shi S (2000) Tsunami deposits. Pure Appl Geophys 157:875–897
Engel M, May S (2012) Bonaire's boulder fields revisited: evidence for Holocene tsunami impact on the Leeward Antilles. Quat Sci Rev 54:126–141
Etienne S, Paris R (2010) Boulder accumulations related to storms on the south coast of the Reykjanes Peninsula (Iceland). Geomorphology 114(1–2):55–70
Etienne S, Buckley M, Paris R et al (2011) The use of boulders for characterizing past tsunamis: lessons from the 2004 Indian ocean and 2009 South Pacific tsunamis. Earth Sci Rev 107(1–2):76–90
Fritz H, Kongko W, Moore A et al (2007) Extreme runup from the 17 July 2006 Java tsunami. Geophys Res Lett 34:12
Ginsburg R (1953) Beachrock in South Florida. J Sediment Res 23(2):85–92
Goff J, Chague-Goff C (2014) The Australian tsunami database: a review. Prog Phys Geogr 38(2):218–240
Goff J, Chagué-Goff C, Nichol S (2001) Palaeotsunami deposits: a New Zealand perspective. Sed Geol 143(1–2):1–6
Goff J et al (2010) Testing the hypothesis for tsunami boulder deposition from suspension. Mar Geol 277(1–4):73–77
Goto K et al (2007) Distribution, origin and transport process of boulders deposited by the 2004 Indian Ocean tsunami at Pakarang Cape. Thail Sediment Geol 202(4):821–837
Goto K, Okada K, Imamura F (2009a) Characteristics and hydrodynamics of boulders transported by storm waves at Kudaka Island. Jpn Mar Geol 262(1–4):14–24
Goto K, Okada K, Imamura F (2009b) Importance of the initial waveform and coastal profile for tsunami transport of boulders. Pol J Environ Stud 18:1
Goto K, Okada K, Imamura F (2010a) Discrimination of boulders deposited by tsunamis and storm waves at Ishigaki Island. Jpn Mar Geol 269(1–2):34–45
Goto K, Okada K, Imamura F (2010b) Numerical analysis of boulder transport by the 2004 Indian Ocean tsunami at Pakarang Cape. Thail Mar Geol 268(1–4):97–105
Goto K, Miyagib K, Kawanac T, Takahashia J, Imamuraa F (2011) Emplacement and movement of boulders by known storm waves—Field evidence from the Okinawa Islands. Jpn Mar Geol 283(1–4):6–78
Goto K et al (2012) Sedimentary processes associated with sand and boulder deposits formed by the 2011 Tohoku-oki tsunami at Sabusawa Island, Japan. Sed Geol 282:188–198
Gunawan E, Widiyantoro S (2019) Active tectonic deformation in Java, Indonesia inferred from a GPS-derived strain rate. J Geodyn 123:49–54
Hall S, Pettersson J, Meservy W, Harris R, Agustinawati D, Olson J, McFarlane A (2017) Awareness of tsunami natural warning signs and intended evacuation behaviors in Java. Indones Nat Hazards 89(1):473–496

Hanifa N et al (2014) Interplate coupling model off the southwestern coast of Java, Indonesia, based on continuous GPS data in 2008–2010. Earth Planet Sci Lett 401:159–171
Harris R (2011) The nature of the Banda Arc–continent collision in the Timor region. In: Brown D, Ryan P (eds) Arc continent collision. Springer, Berlin, Heidelberg, pp 163–211
Harris R, Major J (2016) Waves of destruction in the East Indies: the Wichmann catalogue of earthquakes and tsunami in the Indonesian region from 1538 to 1877. Geological Society London. Spec Pub 441:9–46
Hébert H et al (2012) The 2006 July 17 Java (Indonesia) tsunami from satellite imagery and numerical modelling: a single or complex source? Geophys J Int 191(3):1255–1271
Hogg A et al (2013) SHCal13 Southern Hemisphere calibration, 0–50,000 years cal BP. Radiocarbon 55(4):1889–1903
Ishizawa T et al (2020) Dating tsunami deposits: present knowledge and challenges. Earth Sci Rev 200:102971
Kato Y, Akamine N, Ohori K, Tamaki T, Tamura K (1991) Movement of limestone blocks by wind waves—an example by typhoon no. 21, 1990, at Zanpa Cape, Okinawa Island. Southwest Jpn Proc Uni Ryukyus 51:19–33
Kato Y, Uema K, Yamaoka N (1995) Movement of limestone-blocks by wind waves—an example by typhoon no. 13, 1994 at the south coast of Yonaguni Island, southwestern Japan. Proc Univ Ryukyus 59:29–41
Kennedy AB, Cox R, Dias F (2021) Storm waves may be the source of some "tsunami" coastal boulder deposits. Geophy Res Lett 48(11):e2020GL090775
Koulali A et al (2017) The kinematics of crustal deformation in Java from GPS observations: implications for fault slip partitioning. Earth Planet Sci Lett 458:69–79
Lau A et al (2015) Advantages of beachrock slabs for interpreting high-energy wave transport: evidence from Ludao Island in south-eastern Taiwan. Geomorphology 228:263–274
Lay T et al (2005) The great Sumatra-Andaman earthquake of 26 December 2004. Science 308(5725):1127–1133
Lorang M (2000) Predicting threshold entrainment mass for a boulder beach. J Coast Res 16:432–445
Major J, Harris R et al (2013) Quaternary hinterland evolution of the active Banda Arc: Surface uplift and neotectonic deformation recorded by coral terraces at Kisar, Indonesia. J Asian Earth Sci 73:149–161
Maramai A, Tinti S (1997) The 3 June 1994 Java tsunami: a post-event survey of the coastal effects. Nat Hazards 15(1):31–49
Marriner N, Kaniewski D, Morhange C, Flaux C, Giaime M, Vacchi M, Goff J (2017) Tsunamis in the geological record: making waves with a cautionary tale from the Mediterranean. Sci Adv 3(10):e1700485
Martin SS, Cummins PR, Meltzner AJ (2022) Gempa Nusantara: a database of 7380 macroseismic observations for 1200 historical earthquakes in Indonesia from 1546 to 1950. Bull Seismol Soc Am 112(6):2958–2980
Mastronuzzi G, Sans`o P (2000) Boulders transport by catastrophic waves along the Ionian coast of Apulia (Southern Italy). Mar Geol 170(1–2):93–103
Medina F, Mhammdi N, Chigner A, Akil M, Jaaidi EB (2011) The Rabat and Larache boulder fields; new examples of high-energy deposits related to storms and tsunami waves in north-western Morocco. Nat Hazards 59:725–747. https://doi.org/10.1007/s11069-011-9792-x
Meservy W (2017) Evaluating the east Java tsunami hazard: what can newly discovered imbricate coastal boulder accumulations near Pacitan and at Pantai Papuma, Indonesia Tell Us? MSc. Thesis, Brigham Young University, https://scholarsarchive.byu.edu/etd/6545
Milliman J (1974) Marine carbonates. Springer, Heidelberg
Moore A et al (2011) Sedimentary deposits from the 17 July 2006 Western Java Tsunami, Indonesia: use of grain size analyses to assess tsunami flow depth, speed, and traction carpet characteristics. Pure Appl Geophys 168:1951–1961
Morton R, Gelfenbaum G, Jaffe BE (2007) Physical criteria for distinguishing sandy tsunami and storm deposits using modern examples. Sed Geol 200(3–4):184–207
Mulyana A (2018) Hubungan Penyuluhan Terhadap Pengetahuan Siswa Tentang Penanggulangan Bencana Gempa Bumi Di SMK Bhakti Kencana Tasikmalaya. Jurnal Mitra Kencana Keperawatan Dan Kebidanan 1(2):1–10
Nandasena N, Paris R, Tanaka N (2011a) Numerical assessment of boulder transport by the 2004 Indian Ocean tsunami in Lhok Nga, West Banda Aceh (Sumatra, Indonesia). Comput Geosci 37(9):1391–1399
Newcomb K, McCann W (1987) Seismic history and seismotectonics of the Sunda arc. J Geophys Res Solid Earth 92(B1):421–439

Noormets R, Crook K, Felton E (2004) Sedimentology of rocky shorelines. Hydrodynamics of megaclast emplacement and transport on a shore platform, Oahu, Hawaii. Sediment Geol 172(1–2):41–65
Nott J (1997) Extremely high-energy wave deposits inside the Great Barrier Reef, Australia: determining the cause—tsunami or tropical cyclone. Mar Geol 141(1–4):193–207
Nott J (2000) Records of prehistoric tsunamis from boulder deposits: evidence from Australia. Sci Tsunami Haz 18(1):3–14
Nott J (2003) Tsunami or storm waves: determining the origin of a spectacular field of wave emplaced boulders using numerical storm surge and wave models and hydrodynamic transport equations. J Coast Res 4:348–356
Nott J (2004) The tsunami hypothesis—comparisons of the field evidence against the effects, on the western Australian coast, of some of the most powerful storms on earth. Mar Geol 208(1):1–12
Nott J, Bryant E (2003) Extreme marine inundations (tsunamis?) of coastal western Australia. J of Geology 111(6):691–706
Nugroho H, Harris R, Lestariya A, Maruf B (2009) Plate boundary reorganization in the active Banda Arc–continent collision: insights from new GPS measurements. Tectonophysics 479(1–2):52–65
Oak H (1984) The boulder beach: a fundamentally distinct sedimentary assemblage. Ann Assoc Am Geol 74:71–82
O'Connor S et al (2010) Pre-bomb marine reservoir variability in the Kimberley region. West Aust Radiocarb 52(3):1158–1165
Oetjen J, Engel M, Schüttrump H (2021) Experiments on tsunami induced boulder transport–a review. Earth Sci Rev 220:103714
Paris R, Wassmer P, Lavigne F et al (2014) Coupling eruption and tsunami records: the Krakatau 1883 case study, Indonesia. Bull Volcanol 76(4):1–23
Polet J, Thio H (2003) The 1994 Java tsunami earthquake and its "normal" aftershocks. Geophys Res Lett 30:9
Pradjoko E, Kusuma T, Setyandito O, Suroso A, Harianto B (2015) The tsunami run-up assessment of 1977 Sumba Earthquake in Kuta, Center of Lombok, Indonesia. Proced Earth Planet Sci 1(14):9–16
Prendergast A, Brown N (2012) Far-field impact and coastal sedimentation associated with the 2006 Java tsunami in West Australia. Nat Hazards 60:69–79
Raphael CN (1975) Coastal morphology; Southwest Great Abaco Island. Bahamas Geoforum 6(3–4):237–246
Reimer P et al (2013) IntCal13 and Marine13 radiocarbon age calibration curves 0–50,000 years cal BP. Radiocarbon 55(4):1869–1887
Rizal Y et al (2017) Tsunami evidence in south coast Java, case study: Tsunami deposit along south coast of Cilacap. In: IOP conference series: earth and environmental science. 71(1)
Roeber V, Bricker JD (2015) Destructive tsunami-like wave generated by surf beat over a coral reef during Typhoon Haiyan. Nat Commun 6(1):7854
Russell R (1963) Recent Recession of Tropical Cliffy Coasts: elevated benches and other coastal forms give evidence of eustatic changes in sea level. Science 139(3549):9–15
Russell RJ (1962). Origin of beach rock. Z Geomorphol 61–16.
Saintilan N, Rogers K (2005) Recent storm boulder deposits on the Beecroft Peninsula, New South Wales. Aust Geogr Res 43(4):429–432
Scheffers A (2004) Tsunami imprints on the Leeward Netherlands Antilles (Aruba, Curaçao, Bonaire) and their relation to other coastal problems. Quat Int 120(1):163–172
Scheffers A (2008) Tsunami boulder deposits. In: Shiki T, Yamazaki T, Tsuji Y, Nanayama F (eds) Tsunamiites. Elsevier, Amsterdam, pp 299–317
Scheffers A (2021) Tsunami boulder deposits–a strongly debated topic in paleo-tsunami research. In: Shiki T, Yamazaki T, Tsuji Y, Nanayama F (eds) Tsunamiites. Elsevier, Amsterdam, pp 353–382
Scheffers A, Kelletat D (2003) Sedimentologic and geomorphologic tsunami imprints worldwide—a review. Earth Sci Rev 63(1–2):83–92
Scheffers A, Kinis S (2014) Stable imbrication and delicate/unstable settings in coastal boulder deposits: indicators for tsunami dislocation? Quat Int 332:73–84
Scheffers A, Scheffers S, Kelletat D (2005) Paleo-tsunami relics on the southern and central Antillean Island arc. J Coast Res 21(2):263–273
Schneider B et al (2019) Tsunami and storm sediments in Oman: characterizing extreme wave deposits using terrestrial laser scanning. J Coast Conserv 23:801–815
Scoffin T (1993) The geological effects of hurricanes on coral reefs and the interpretation of storm deposits. Coral Reefs 12:203–221
Shah-Hosseini M, Morhange C, Beni AN, Marriner N, Lahijani H, Hamzeh M, Sabatier F (2011) Coastal boulders as evidence for high-energy waves on the Iranian coast of Makran. Mar Geol 290:17–28. https://doi.org/10.1016/j.margeo.2011.10.003

Soria JLA, Switzer AD, Pilarczyk JE, Tang H, Weiss R, Siringan F, Manglicmot M, Gallentes A, Lau AA, Cheong AYL, Koh TWL (2018) Surf beat-induced overwash during Typhoon Haiyan deposited two distinct sediment assemblages on the carbonate coast of Hernani, Samar, central Philippines. Mar Geol 396:215–230
Southon J et al (2002) Marine reservoir corrections for the Indian Ocean and Southeast Asia. Radiocarbon 44(1):167–180
Suanez S, Fichaut B, Magne R (2009) Cliff-top storm deposits on Banneg Island, Brittany, France: effects of giant waves in the eastern Atlantic Ocean. Sed Geol 220(1–2):12–28
Sulaeman H (2018) Discovery of paleotsunami deposits along the eastern Sunda Arc: potential for megathrust earthquakes in Bali, MSc. Thesis, Brigham Young University, https://scholarsarchive.byu.edu/etd/
Switzer AD, Burston JM (2010) Competing mechanisms for boulder deposition on the southeast Australian coast. Geomorphology 114(1–2):42–54
Switzer A, Jones B (2008) Large-scale washover sedimentation in a freshwater lagoon from the southeast Australian coast: sea-level change, tsunami or exceptionally large storm? Holocene 18(5):787–803
Synolakis C, Imamura F, Tsuji Y et al (1995) Damage, conditions of East Java tsunami of 1994 analyzed. EOS Trans Am Geophys Union 76(26):257–257
Szczucinski W (2012) The post-depositional changes of the onshore 2004 tsunami deposits on the Andaman Sea coast of Thailand. Nat Hazards 60:115–133
Titov V, Moore C, Greenslade D et al (2011) A new tool for inundation modeling: community modeling interface for tsunamis (commit). Pure Appl Geophys 168(11):2121–2131
Titov V, Kˆanoˇglu U, Synolakis C (2016) Development of MOST for real-time tsunami forecasting. Ph.D. thesis, American Society of Civil Engineers.
Tsuboi S (2000) Application of mwp to tsunami earthquake. Geophys Res Lett 27(19):3105–3108
Tsuji Y, Imamura F, Matsutomi H et al (1995a) Field survey of the east Java earthquake and tsunami of June 3, 1994. In: Imamura F, Satake K (eds) Tsunamis: 1992–1994. Springer, Berlin, pp 839–854
Tsuji Y et al (1995b) Field survey of the East Java earthquake and tsunami of June 3, 1994. In: Imamura F, Satake K (eds) Tsunamis: 1992–1994: their generation, dynamics, and hazard. Birkhäuser, Basel
Vieira M, Fernando De Ros L, Bezerra F (2007) Lithofaciology and palaeoenvironmental analysis of Holocene beachrocks in northeastern Brazil. J Coast Res 23(6):1535–1548
Vött A et al (2019) Publicity waves based on manipulated geoscientific data suggesting climatic trigger for majority of tsunami findings in the Mediterranean-Response to "Tsunamis in the geological record: making waves with a cautionary tale from the Mediterranean" by Marriner et al.(2017). Zeitschrift für Geomorphologie 62(2):7–45
Vousdoukas M, Velegrakis A, Plomaritis T (2007) Beachrock occurrence, characteristics, formation mechanisms and impacts. Earth Sci Rev 85(1–2):23–46
Wichmann A (1918) Die Erdbeben des indischen Archipels bis zum Jahre 1857, vol 20. Koninklijke Akademie van Wetenschappen, Amsterdam
Wichmann A (1922) Die Erdbeben des Indischen Archipels von 1858 bis 1877. Koninklijke Akademie van Wetenschappen, Amsterdam
Windupranata W et al (2019) Impact analysis of Tropical Cyclone Cempaka-Dahlia on wave heights in Indonesian waters from numerical model and altimetry satellite. In: KnE Engineering pp 203–214
Xia Y et al (2021) Marine forearc structure of eastern Java and its role in the 1994 Java tsunami earthquake. Solid Earth 12(11):2467–2477

Authors and Affiliations

R. Harris[1] · W. Meservy[1] · H. Sulaeman[1] · M. Bunds[2] · J. Andreini[2] · B. Sharp[1] · B. Berrett[3] · J. Whitehead[4] · G. Carver[4] · G. Setiadi[5] · S. Hapsoro[5] · C. Prasetyadi[5]

✉ R. Harris
rharris@byu.edu

[1] Geological Sciences, Brigham Young University, Provo, UT 84602-4606, USA

[2] Geology, Utah Valley University, Orem, UT, USA

[3] Civil Engineering, Oregon State University, Corvallis, OR 97331, USA

[4] Mathematics, Brigham Young University, Provo, UT 84602, USA

[5] Geological Sciences, Universitas Pembangunan Nasional Yogyakarta, Yogyakarta, Indonesia